LANGMUIR

pubs.acs.org/Langmuir Article

Degradable Anti-Biofouling Polyester Coatings with Controllable Lifetimes

Gaoyan Mu, Jan Genzer, and Christopher B. Gorman*

Cite This: *Langmuir* 2022, 38, 1488−1496 Read Online

ACCESS | Metrics & More | Article Recommendations | Supporting Information

ABSTRACT: To achieve degradable, anti-biofouling coatings with longer lifetimes and better mechanical properties, we synthesized a series of degradable co-polyesters composed of cyclic ketene acetals, di-(ethylene glycol) methyl ether methacrylate, and a photoactive curing agent, 4-benzoylphenyl methacrylate, using a radical ring-opening polymerization. The precursor co-polyesters were spin-coated on a benzophenone-functionalized silicon wafer to form ca. 60 nm films and drop-casted on glass to form ∼32 μm films. The copolymers were cross-linked via UV irradiation at 365 nm. The degradation of films was studied by immersing the specimens in aqueous buffers of different pH values. The results show that both the pH of buffer solutions and gel fractions of networks affect the degradation rate. The coatings show good bovine serum albumin resistance capability. By adjusting the fractions of monomers, the degradation rate and degree of hydration (e.g., swelling ratio) are controllable.

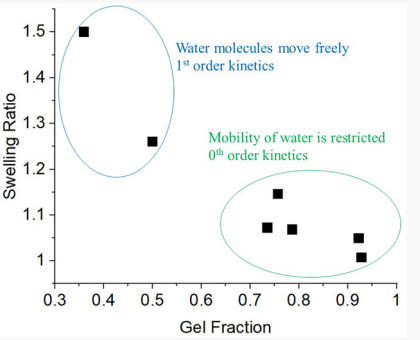

INTRODUCTION

Biofouling has always been a major issue in marine and medical applications. Biomass adsorbed on ship hulls generates high frictional resistance, adding to the cost of transportation and travel. Biofouling also reduces the efficacy of biomedical implants and biosensors, and it also contributes to infections.[1−3] The first step of biofouling is the non-specific adsorption of protein on surfaces.[4] Numerous researchers invented various anti-biofouling coatings to resist protein adsorption. These include poly(ethylene glycol) (PEG)-based coatings,[5] fouling release coatings,[6−8] zwitterionic polymer coatings,[9,10] amphiphilic polymer coatings,[11] and polymer brushes[12] on surfaces of materials. Although those static coatings could resist protein adsorption to some extent, the protein will eventually adsorb on the surfaces. To solve this problem, we synthesized novel, dynamic coatings based on degradable polyester networks. We assumed that the adsorbed protein would be released with the degradation of the coatings. From our previous work, those dynamic (e.g., degradable) coatings resist protein adsorption better than similar, non-dynamic coatings within their lifetime.[13]

However, the lifetimes of those previously reported coatings are short due to fast degradation.[13] Moreover, they could be prepared with only limited thickness, and they had poor mechanical properties, likely from their low molecular weight.[14−18] We synthesized new polyesters with a lower ester ratio in their backbone and with higher molecular weights to solve those problems. Compared with ring-opening polymerization (ROP) of epoxides and anhydrides, polyesters synthesized by radical ring-opening polymerization (RROP) have higher molecular weights.

EXPERIMENTAL SECTION

Materials. Chloroacetaldehyde dimethyl acetal, diethylene glycol, ethylene glycol, *p*-toluenesulfonic acid, *tert*-butyl alcohol, silver nitrate, potassium *tert*-butoxide, 18-crown-6, methacryloyl chloride, 4-hydroxyl benzophenone, allyl bromide, potassium carbonate, triethoxysilane, platinum/carbon, magnesium sulfate, di-(ethylene glycol) methyl ether methacrylate (EGMMA), poly(vinylpyrrolidone) (PVP), copper(II) chloride, bicinchoninic acid (BCA) assay kit, potassium dihydrogen phosphate, potassium phosphate dibasic, sodium hydroxide, hydrochloride acid, bovine serum albumin (BSA), and albumin-fluorescein isothiocyanate conjugate (fluorescent BSA) were purchased from Sigma-Aldrich (St. Louis, MO, USA). All solvents were obtained from VWR (Atlanta, GA, USA). Silicon wafers were purchased from ePAK International Inc. (Austin, TX, USA).

Instrumentation. All monomers and polymers were characterized by proton nuclear magnetic resonance (^{1}H NMR, 400 MHz) spectroscopy and carbon-13 nuclear magnetic resonance (^{13}C NMR, 100 MHz) spectroscopy (Varian USA or Bruker USA). The silicon wafers were cleaned using a UVO-cleaner (model no. 42, Jelight Company, Inc. 2 Mason, Irvine, CA, USA). The polymer films were deposited by a spin coater (PNM32 model, Headway Research, Inc., USA). The molecular weights of polymers were determined by size exclusion chromatography (SEC), Shimadzu 2.0. (Shimadzu Corporation, Columbia, MD, USA), equipped with light scattering and refractive index detectors (Wyatt) at a flow rate of 0.5 mL/min in THF with polystyrene as the standard. The thickness of thin films was

Received: October 22, 2021
Revised: December 29, 2021
Published: January 20, 2022

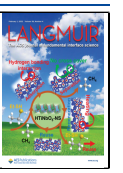

https://doi.org/10.1021/acs.langmuir.1c02822
Langmuir 2022, 38, 1488−1496

Scheme 1. Radical Ring-Opening Polymerization

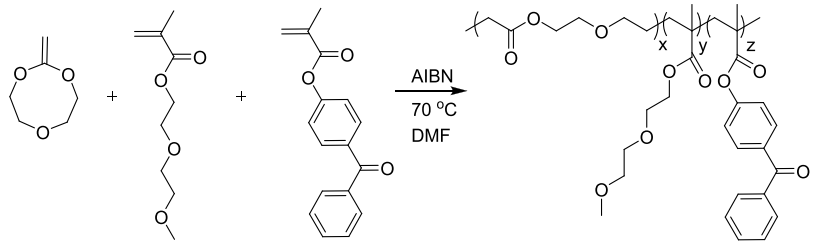

detected by variable-angle spectroscopic ellipsometry (VASE, J.A. Woollam). An Omnicure series-1000 UV lamp activated the photo active-cross-linking reactions at a wavelength of 365 nm (Lumen Dynamics, USA). The UV light intensity was examined by an ILT1400-A radiometer/photometer (International Light Technology). The coatings containing fluorescent BSA were observed under an Olympus BX61 fluorescence microscope (Olympus). The water contact angles were measured using a Ramé Hart contact angle goniometer (model no. 100-00, Succasunna, NJ) equipped with a liquid dispenser, camera, and image-processing software. A drop of DI water with a volume of ~5 μL was placed on the wafer, and the static contact angles were measured. The average contact angle was determined over 3−5 measurements. The mechanical properties and glass transition temperatures of drop-coating films were measured by a TA instrument DMA 850. The absorbances of BCA assay solutions were measured by a Cary 60 UV−vis spectrometer (Agilent Technologies). The thicknesses of drop-casted films on glass slides were measured using a Tencor P-7 stylus profiler (KLA Corporation). A small piece of film (1 mm × 3 mm) was cut off from each specimen to create the bare part as a reference for profilometry. By setting the bare thickness as 0, the thickness of the remaining films were measured.

Synthesis of 2-methylene-1,3,6-trioxocane Cyclic Ketene Acetal (CKA). A total of 28 mL of diethylene glycol (0.30 mol) and 34 mL of chloroacetaldehyde dimethyl acetal (0.30 mol) were mixed in a 250 mL round bottom flask equipped with a 10 cm Vigreaux column. *p*-Toluenesulfonic acid (75 mg, 0.43 mmol) was added to the flask. The reaction was heated at 115 °C for 4 h. After the calculated amount of methanol (0.6 mol, 24 mL) was collected, the reaction was cooled. The crude product was distilled under vacuum (60 °C, 1 torr) to get 21.1 g (0.13 mol) 2-(chloromethyl)-1,3,6-trioxocane, which formed crystals as the material cooled to room temperature. (43% yield). ^{1}H NMR (400 MHz; $CDCl_3$): δ 7.26 (s, $CDCl_3$), 4.79 (t, 1H), 3.98 (m, 4H), 3.76 (m, 4H), and 3.48 (d, 2H). ^{13}C NMR (100 MHz; $CDCl_3$): δ 106.3, 77.2 ($CDCl_3$), 73.8, 71.8, and 45.3.

A total of 16.7 g (0.1 mol) of 2-(chloromethyl)-1,3,6-trioxocane and 1.2 g of 18-crown-6 (4.5 mmol) were dissolved in 30 mL *tert*-butyl alcohol in a 250 mL round bottom flask. A total of 9.6 g (87 mmol) of potassium *tert*-butoxide was added into the flask slowly. The reaction was refluxed overnight at 110 °C. After cooling down, the crude product was centrifuged at 2500 rpm for 5 min. The supernatant liquid was collected, and *tert*-butyl alcohol was removed by rotatory evaporation. The residue was fractionated twice through a 10 cm Vigreaux column (50 °C, 1 torr) to give 4.0 g (0.031 mol) of 2-methylene-1,3,6-trioxocane as clear liquid (43% yield). ^{1}H NMR (400 MHz; $CDCl_3$): δ 7.26 (s, $CDCl_3$), 4.06 (t, 4H), 3.79 (t, 4H), and 3.67 (s, 2H). ^{13}C NMR (100 MHz; $CDCl_3$): δ 163.4, 77.2 ($CDCl_3$), 71.0, 70.4, and 70.3.

Synthesis of 4-Benzoylphenyl Methacrylate (BPMA). A total of 3.97 g (20 mmol) of 4-hydroxybenzophenone and 3.1 mL (22 mmol) of triethylamine were dissolved in DCM (40 mL) in a 250 mL round bottom flask. A total of 2.17 mL (22 mmol) of methacryloyl chloride was dissolved in 23 mL DCM and added dropwise to the flask at 0 °C. The reaction mixture was stirred at 0−5 °C for 4 h. The precipitated triethylammonium chloride was filtered off, and the residue reaction solution was washed twice with 1 M HCl solution, a saturated aqueous $NaHCO_3$ solution, and deionized water. The extracted organic phase was dried with anhydrous magnesium sulfate, and the solvent was removed by a rotary evaporator to yield 4.4 g (17 mmol) 4-benzoylphenyl methacrylate (BPMA) as a white solid. (83% yield) ^{1}H NMR (400 MHz; $CDCl_3$): δ 7.89 (d, 2H), 7.81 (d, 2H), 7.61 (t, 1H), 7.50 (t, 2H), 7.27 (s, $CDCl_3$), 7.26 (d, 2H), 6.40 (s, 1H), 5.82 (s, 1H), and 2.09 (s, 3H). ^{13}C NMR (100 MHz; $CDCl_3$): δ 195.7, 165.5, 154.3, 137.7, 135.7, 135.1, 132.6, 131.8, 130.11, 128.5, 128.1, 121.7, 77.2 ($CDCl_3$), and 18.5.

Radical Ring-Opening Co-Polymerization of CKA, EGMMA, and BPMA. The example described here is the polymer with 7.5% BPMA. For other BPMA content samples, the ratio of monomers was adjusted (Scheme 1). A total of 0.41 mL (2.2 mol) of di-(ethylene glycol) methyl ether methacrylate (EGMMA), 85 mg (0.32 mol) of 4-benzoylphenyl methacrylate (BPMA), and 60 mg (37 mmol) of azobisisobutyronitrile (AIBN) were dissolved in 3 mL of dimethylformamide (DMF) in a 50 mL Schlenk flask equipped with a stir bar. Then, 0.30 mL (1.9 mol) of freshly distilled 2-methylene-1,3,6-trioxocane was added into the flask with cooling. The Schlenk flask was immersed in liquid nitrogen for 5 min to freeze the solvent. The gas in the flask was removed by vacuum for 8 min. The frozen solution thawed by a water bath following by stirring under nitrogen for 1 min. This degassing process was repeated three times. The mixture was stirred and maintained at 70 °C for 3 days. Upon completion, the solvent was removed by rotatory evaporation. A few drops of dichloromethane (DCM) were added, and the solution was precipitated into 20 mL diethyl ether. The polymer was collected after centrifugation and dried under a high vacuum overnight. For all samples, the product was a clear, viscous liquid (97% yield). ^{1}H NMR (400 MHz; $CDCl_3$): δ 7.81 (m, 4H), 7.55 (m, 3H), 7.27 (s, $CDCl_3$), 6.96 (m, 2H), 4.28 (m, 4H), 3.79 (t, 2H), 3.70 (t, 2H), 3.63 (t, 3H), 3.55 (t, 3H), 3.39 (s, 3H), 2.44 (m, 2H), 2.10 (s), 1.94 (m), and 1.20 (m, 6H). ^{13}C-NMR (100 MHz; $CDCl_3$): δ 195.4, 177.5, 171.2, 138.1, 132.9, 131.9, 129.7, δ 128.2, 118.3, 115.1, 114.0, 77.2 ($CDCl_3$), 72.4, 72.0, 70.6, 69.1, 68.9, 68.6, 64.0, 63.6, 61.9, 61.7, 59.1, 53.5, 44.7, 43.9, 26.7, 21.0, 18.7, 16.9, 15.0, and 13.8.

Preparation of Spin-Coated Polyester Network Films and Degradation Study. 4-[3-(Triethoxysilyl)propyloxy]-benzophenone (TESPBP) was synthesized as described previously.[13] Freshly prepared TESPBP were dissolved in toluene and spin-coated onto a UVO-cleaned silicon wafer (1500 rpm, 45 s spinning). Then, the sample was annealed in the oven overnight at 110 °C followed by extraction in toluene and drying under N_2 gas. A functionalized silicon wafer coated with 2−3 nm of TESPBP was obtained. Polyester samples were dissolved in dry dioxane and filtered through a 0.2 μm PTFE membrane to prepare a 20 mg/mL stock solution. The polymer solutions were then spin-coated onto the TESPBP-functionalized silicon wafer (2500 rpm, 30 s spinning). The prepared layer was illuminated with UV light at 365 nm with a dosage of 30 mW/cm^2 for 5 min. The specimen was then extracted with THF overnight to remove any uncross-linked polymer from the substrate leaving the cross-linked polyester network attached to the substrate (60−75 nm). The degradation study followed the procedure provided previously.[13]

Preparation of Drop-Casted Polyester Network Films and Degradation Study. Polyesters were dissolved in distilled THF and filtered through a 0.2 μm PTFE membrane to prepare 50 mg/mL stock solution. The stock solutions were drop-casted on the clean glass slides and placed in vacuum oven at 60 °C for 5 h. Then, the specimens were moved out and irradiated under UV light at 375 nm with a dosage of 40 mW/cm^2 for 3 h. After washing with methanol,

https://doi.org/10.1021/acs.langmuir.1c02822
Langmuir 2022, 38, 1488−1496

drop-cast films (~32 μm) were prepared. The degradation of drop-cast films on glass was studied by the thickness change of samples immersed in PBS solution with various pH values (6.4, 7.0, 7.4, 8.2). The PBS solution was prepared using potassium dihydrogen phosphate and potassium phosphate dibasic with 1 M ionic strength. The drop-casted films on glass substrates were immersed in PBS solutions in 20 mL vials and placed on the shaker at 200 rpm. Wafers were taken out of the buffer solution at specific time points, washed by DI water, and dried with N_2 gas, and the film thickness was measured via profilometry.

Bicinchoninic Acid (BCA) Protein Assay. The BSA adsorbed on drop-casted films were quantified by a BSA protein assay as described previously.[19] After immersion in BSA solution, two samples were inserted in a designed thin layer cell. The cell was filled with 5 wt % aqueous sodium dodecyl sulfate (SDS) solution. The adsorbed BSA was removed by sonication for 30 min. The BSA concentration of the collected solution was measured using a commercial BCA assay kit. The working solution was prepared by mixing reagent A (3 mL) and reagent B (60 μL) with a ratio of 50:1. A 150 μL aliquot of the collected protein solution was added to 3 mL of the working solution and then incubated at 37 °C for 30 min. The absorption of the solution at 562 nm was measured using a UV−vis spectrometer. The BCA assay standard calibration curve at 562 nm is shown in Figure S12.

The measurements of gel fraction, protein adsorption, hydrophilicity, and hydration followed the procedures provided in the literature.[13]

RESULTS AND DISCUSSION

The cyclic ketene acetal (CKA) 2-methylene-1,3,6-trioxocane was chosen to provide a hydrophilic and degradable backbone as the polymerization of this monomer leads to ester linkages in the backbone.[20] Di-(ethylene glycol) methyl ether methacrylate (EGMMA) was chosen as a comonomer to improve hydrophilicity of the side chain and to retard protein adsorption in the short term. A second methacrylate, 4-benzoylphenyl methacrylate (BPMA), was utilized as a promiscuous UV cross-linker (Scheme 1).[21] A benzophenone-functionalized silicon wafer was used to covalently anchor the polymer to the surface during the UV cross-linking step. In the absence of this functionality, the polyester does not attach stably on the silicon surface. Thin films ca. 60 nm and 32 μm were prepared by spin-coating and drop-casting, respectively. Both coated polyesters were cross-linked to form networks after 370 nm UV irradiation. The degradation and anti-fouling capabilities of those films were investigated.

Reactivity Ratios. Co-polyesters with different fractions of monomers were synthesized. However, the structure of the monomers are sufficiently different, so the reactivity ratios were calculated. To do this, the mole fractions of monomers in polymers were determined by ^{1}H NMR integration as described in the Supporting Information. A total of nine samples were prepared. These monomer reactivity ratios are defined as:

$$r_{12} = \frac{k_{11}}{k_{12}},$$

$$r_{13} = \frac{k_{11}}{k_{13}},$$

$$r_{21} = \frac{k_{22}}{k_{21}},$$

$$r_{23} = \frac{k_{22}}{k_{23}},$$

$$r_{31} = \frac{k_{33}}{k_{31}},$$

$$r_{32} = \frac{k_{33}}{k_{32}}$$

where r represents the reactivity ratio and k refers to the rate constant.

The feed ratios and mole fractions in polymers are summarized in Table 1. Although the calculation of reactivity ratios for copolymers composed of two monomers is relatively straightforward, a terpolymer system is more complex. Reactivity ratios of each of the monomers were calculated using equations from the literature.[22−25] Because it was not possible to obtain analytical fits to the system of equations, a Monte Carlo-based simulated annealing fitting routine was constructed and used. The procedure of calculating the reactivity ratios is described in Supporting information (Figure S15). The average reactivity ratios of 15 sets were:

$$r_{12} = 0.0460 \pm 0.0250,$$

$$r_{13} = 0.361 \pm 0.190,$$

$$r_{21} = 10.9 \pm 0.8,$$

$$r_{23} = 28.1 \pm 2.1,$$

$$r_{31} = 0.311 \pm 0.125,$$

$$r_{32} = 0.0273 \pm 0.0116$$

The results indicate EGMA prefers to react with itself while CKA and BPMA prefer to react with either of the other monomers. These values also allow us to control the composition of the polymers by varying the monomer feed ratios.

Table 1. Feed Ratios and Mole Fractions in Polymers[a]

sample	f1	f2	f3	F1	F2	F3
1	0.01	0.3	0.69	0.031	0.62	0.349
2	0.02	0.1	0.88	0.034	0.675	0.291
3	0.01	0.513	0.471	0.089	0.737	0.235
4	0.01	0.513	0.471	0.095	0.773	0.132
5	0.075	0.49	0.435	0.125	0.62	0.248
6	0.038	0.472	0.489	0.094	0.783	0.123
7	0.05	0.5	0.45	0.074	0.735	0.191
8	0.035	0.476	0.489	0.044	0.771	0.185
9	0.2	0.5	0.3	0.159	0.628	0.213

[a]f1, f2, f3 represent the feed ratios of BPMA, EGMA, and CKA. F1, F2, and F3 represent the mole fractions of BPMA, EGMA, and CKA in copolymers.

https://doi.org/10.1021/acs.langmuir.1c02822
Langmuir 2022, 38, 1488−1496

Molecular Weights. The number-average molecular weights, weight-average molecular weights, and PDI of polymers were measured by size-exclusion chromatography (SEC) with polystyrene standards as the reference. The molecular weights are in a range of 30 to 50 kDa, which are much higher than the polyesters achieved by ring-opening polymerization of epoxides and anhydrides (ca. 4 KDa) previously (Table 2).

Table 2. Molecular Weights of Polyesters

sample	M_n (kg/mol)[a]	M_w (kg/mol)[a]	PDI
1	34.8	59.8	1.69
2	30.9	51.8	1.68
3	38.6	66.9	1.73
4	40.5	106	2.61
5	29.5	67.3	2.28
6	31.8	57.1	1.80
7	51.6	99.9	1.93
8	33.2	62.3	1.88
9	32.5	59.5	1.83

[a]Based on SEC measurements versus polystyrene standards.

Surface Attached Networks. We and others have previously used benzophenone (BP)-containing units to promiscuously cross-link and covalently anchor polymer layers to surfaces.[13,21,26] Under UV irradiation, the BP units form triplet C•−O• bi-radicals. Those radicals abstract an adjacent hydrogen atom, creating two carbon-based radicals (C•−C•), which combine to form a covalent C−C linkage both between polymer chains and with the surfaces, forming surface-bound networks as described previously.[13,21,26] With the same strategy, the polyester with BP units were coated onto the glass slides and cross-linked by UV irradiation. After measuring their thicknesses, the specimens were incubated in tetrahydrofuran (THF) overnight to wash off the uncross-linked material. After drying the specimens, the thicknesses were measured again to determine their gel fraction. The relationship between gel fraction and UV irradiation time is shown in Figure S9. The gel fraction increases with BP fraction in the polymer at a constant UV dose. The polyesters were also drop-casted on glass substrates followed by UV irradiation to make films that were ∼32 μm thick. The specimens were then washed with methanol. The gel fraction of drop-casting film with 5% cross-linker was 0.87. The processes are illustrated in Figure 1.

Degradation of Networks. A previous work showed that the degradation of polyester films is affected by pH and gel fraction.[13,27] The degradation of drop-cast and spin-coated films with different gel fractions in buffer solution with different pH values was studied. Specimens with different gel fractions were immersed in PBS solution with various pH values taken out, and their thicknesses were measured. The thickness of spin-coated films were measured by VASE, and the thickness of drop-cast films was measured by profilometry. Figure 2 shows the percentage thickness change versus time of spin-coated films. The percentage change in thickness was calculated by h_t/h_0 where h_t represents thickness at each specific time, and h_0 is the initial thickness before extraction with THF.

The data in Figure 2 indicate that the degradation rate of the networks increases with increasing pH. Base-catalyzed hydrolysis of the polyester backbone is the most likely mechanism of degradation. To further characterize the degradation products, 5 mg of polyester was dissolved in 10% NaOH solution for 1 day. After the completion, the residue was analyzed by ^{1}H NMR. The ester signals at 2.1 and 4.26 ppm disappeared (Figure S10). This observation is consistent with base-catalyzed hydrolysis of the ester backbone consistent with reports of the degradation of similar polyesters.[13] Therefore, it is reasonable that the degradation rate increases when the pH increases from 6.4 to 8.2.

The data in Figure 2 also indicates that the degradation is slower for higher gel fraction networks. After fitting those data to the function, we found that the rates of the decrease of film thickness were closer to exponential at gel fractions of 0.36, 0.50, and 0.73, while closer to linear at a gel fraction of 0.88. The exponential decrease is a hallmark of first-order kinetics, while a linear decrease is a hallmark of zeroth-order kinetics.

First-order kinetics:

$$-\frac{dh}{dt} = k_1 \times h \tag{1}$$

which, integrated, gives

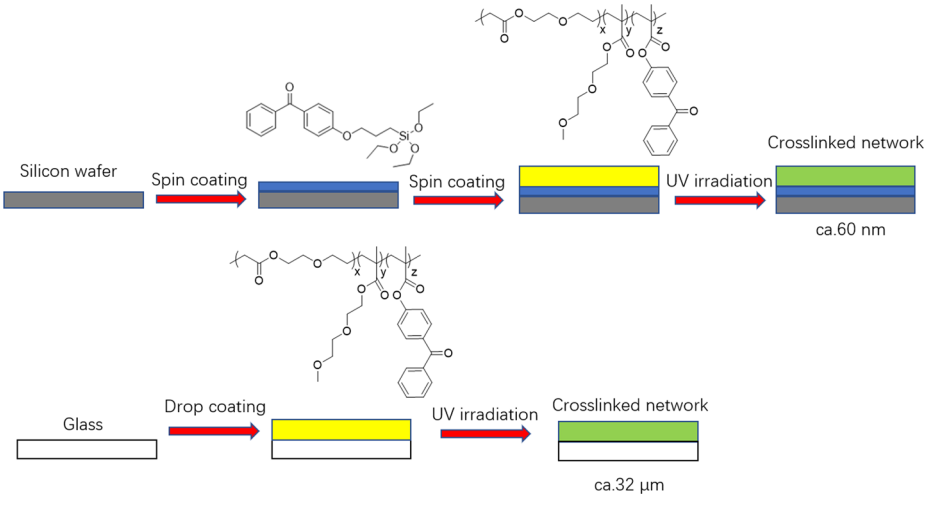

Figure 1. Cartoon illustrating the formation of spin-coated film and drop-casted film.

https://doi.org/10.1021/acs.langmuir.1c02822
Langmuir 2022, 38, 1488−1496

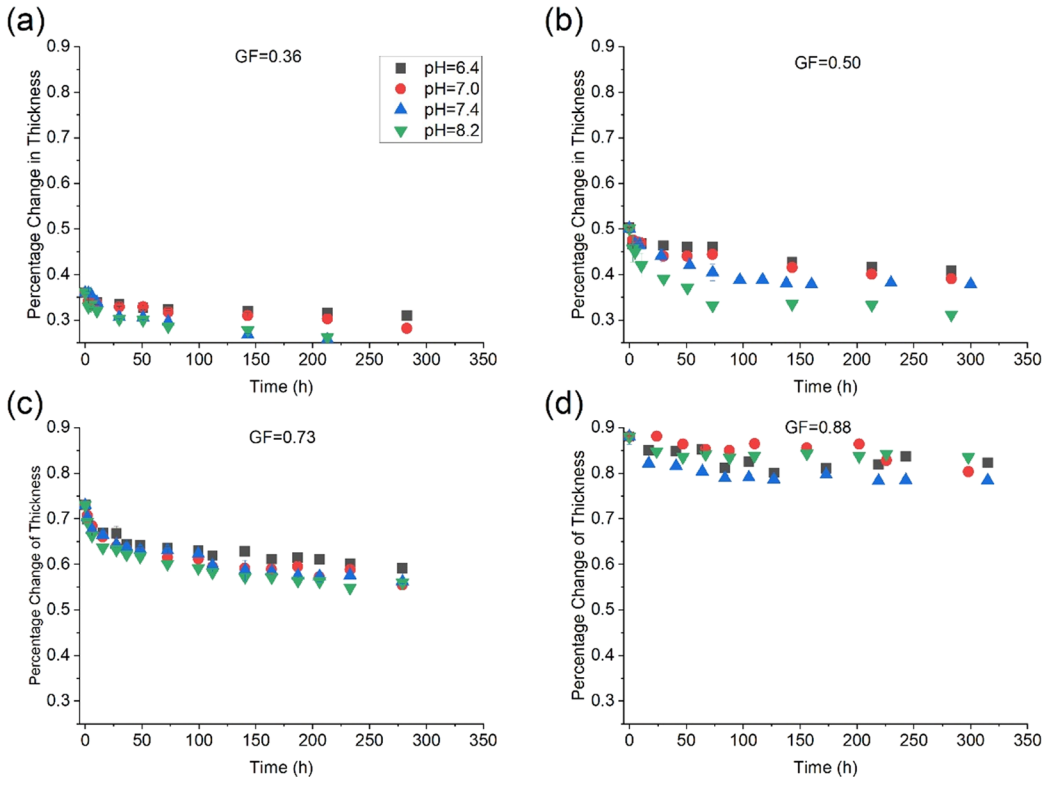

Figure 2. Plots showing the percentage change of thickness of samples of surface-anchored, cross-linked polymers with different gel fractions (GF = 0.36, 0.50, 0.73, 0.88) in PBS buffer solution (ionic strength = 1 M) with various pH values. Thicknesses were determined via ellipsometry. Initial thicknesses of the films varied between 60 and 65 nm. The initial percentage change of thickness is the gel fraction for each sample. All data points were the average values of three measurements on different locations of the same sample, and error bars represent one standard deviation of the average. Many error bars were smaller than the size of the plot symbols.

$$h_t = h_0 \times e^{-k_1 t} \tag{2}$$

Zeroth-order kinetics:

$$-\frac{dh}{dt} = k_0 \tag{3}$$

which, integrated, gives

$$h_t = h_0 - k_0 t \tag{4}$$

h_0 is the thickness at time zero, h_t is the thickness at time t, k_1 is first-order rate constant, and k_0 is zeroth-order rate constant.

Consistent with our previous study, there are two reasons for this trend.[13] First, there is a higher chance for lower gel fraction networks releasing a segment compared with higher gel fraction networks if the same number of ester backbone cleavages. Second, water molecules hydrolyze the network with a low gel fraction more extensively and carry the degraded segments out more efficiently. In contrast, the degradation of high gel fraction networks was restricted to take place on the surface. Therefore, the degradation is faster for lower gel fraction networks and follows first-order kinetics, while slower for higher gel fraction networks and follows zeroth-order kinetics. The hydration of the low gel fraction networks is not as large as the previous films, which makes the degradation across the whole network partially restricted. The slower degradation is also attributed to a smaller number of cleavable ester bonds in the backbone and poorer hydration. Therefore, the lifetime of films is longer due to slow degradation. For lower gel fraction (ca. 0.50), the lifetime of the film in pH 8.2 PBS solution is over 300 h. This behavior compares to only an 8 h lifetime for films reported previously.[13] For higher gel fraction (ca. 0.88), the lifetime of previously reported films[13] was 40 h in pH 8.2 PBS solution. The films reported here only degrade by 5% after 300 h, meaning the lifetimes of the coatings are much longer.

Degradation of drop-cast samples was also investigated. The thickness of these films was characterized by profilometry. The polyester with 5% BPMA was drop-casted to make three films that were ca. 32 μm thick, and the films were immersed in PBS solution with pH values of 6.4, 7.0, and 8.2, respectively. The percentage thickness changes versus immersion time plot is shown in Figure 3. The plot indicates that the thicknesses of films were invariant after 10 days immersion in pH 6.4 and 7.0 PBS solution and only decrease 9% in pH 8.2 PBS solution. It means that the thicker films made by drop-casting dramatically improve the lifetime compared with 60 nm spin-coated samples, but they still degrade.

Protein Adsorption. The extent of protein adsorption on these films was studied using stock solutions with different BSA concentrations and ionic strengths.[28] The effects of ionic strength on BSA adsorption have been discussed.[13,29] Under the first set of conditions, a 1 mg/mL albumin-fluorescein isothiocyanate conjugate protein in phosphate-buffered saline (PBS) with a pH of 7.4 and a total ionic strength of 1 M was employed. Under these conditions, the amount of protein adsorbed on the surfaces is too small to be quantified by a thickness change. Instead, the wafers were taken out of the protein solution at various times and observed under a fluorescence microscope. The amount of BSA adsorbed was quantified by integrating the fluorescence intensity of a fixed

https://doi.org/10.1021/acs.langmuir.1c02822
Langmuir 2022, 38, 1488−1496

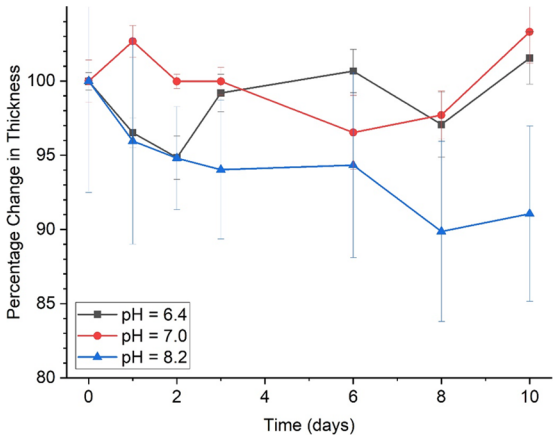

Figure 3. Degradation of drop-cast films in PBS solutions. All data points were the average values of three measurements on different locations of the same sample, and error bars represent one standard deviation of the average.

area in each of the images. Figure S13 shows fluorescent BSA adsorbed on a thin film with a 7.5% feed ratio of BPMA after immersing in stock solutions for 17, 65, 86, and 256 h.

By integrating the fluorescence intensity of each image, intensity versus time plots were constructed (Figure 4). The

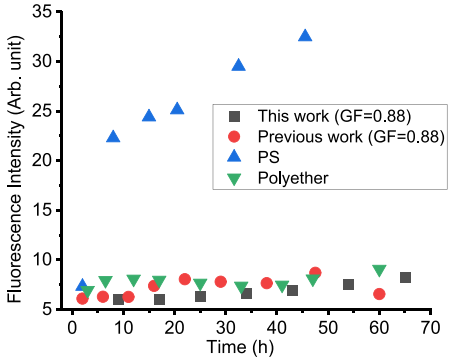

Figure 4. Plot showing fluorescence intensity of thin films of this work, previous work, polystyrene, and polyether immersed in a stock solution with a pH of 7.4, ionic strength of 1 M, and 1 mg/mL fluorescently-labeled BSA at specific immersion times. The red circles are data taken from reference 13. GF denotes gel fraction.

adsorption of BSA on the film with a gel fraction of 0.88 was compared with a polyester previously reported, polystyrene, and a polyether. The structure of polyether is shown in Figure S11. It has a similar structure to the polyesters synthesized in this work but has a non-degradable ether backbone, which permits a reasonable comparison of the protein resistance between chemically similar, static, and dynamic surfaces. The result indicates that the film synthesized in this work has similar protein resistance ability compared to films prepared previously and films of the analogous polyether. All of these films resist protein adsorption better than polystyrene. Hydrophobic interactions between protein and surfaces drive protein adsorption. The backbone and ethylene glycol side chain in this polyester improve the hydrophilicity of the film. It is easier to form a hydration layer on these surfaces and resist protein adsorption. Although this film has lower hydrophilicity and slower degradation compared to those reported previously, it does not affect the resistance to protein adsorption under these conditions. Under these conditions, a dynamic surface does not display an advantage because protein adsorption is so minimal.

In the second set of conditions, a 3 mg/mL BSA solution in phosphate-buffered saline (PBS) with a pH of 7.4 and a total ionic strength of 100 mM was employed. BSA adsorption is more facile with a higher concentration and a lower ionic strength than in the first set of conditions. Films with 1, 2, 3.5, and 5% BPMA were prepared. For each BPMA ratio, two specimens were prepared. One was incubated in PBS solution, and another was incubated in the BSA stock solution for comparison. The two wafers agitated under identical conditions and for the same periods. Both specimens were removed at the same time, and their ellipsometric thicknesses were measured. In Figure 5, the black line indicates the thickness of the specimen incubated in PBS solution at various total immersion times. The red line indicates the thickness of the specimen incubated in PBS-BSA solution. The blue line, achieved by subtracting the black line from the red line, represents the net, adsorbed BSA thickness. It is assumed that the BSA do not affect the degradation of the films. All the specimens resist BSA very well for at least 50 h. The specimen with a 5% BPMA ratio adsorbed more BSA. There are several possible reasons for this behavior. First, the hydrophobic BPMA will increase the hydrophobic interaction between BSA and the surface. Second, the networks with higher BPMA ratios and thus higher gel fractions degrade slower. Degradation may have less of a role in resisting any adsorbed protein. Third, the hydration of the film decreases with increasing gel fraction. The effects of hydration on protein adsorption will be discussed later.

For comparison, the films of polystyrene, the polyether, and polyesters previously reported[13] with similar gel fraction (0.8) were prepared and incubated in PBS-BSA solution, as well as the film of the polymer synthesized in this work. Figure 6 indicates that the BSA starts to grow on PS surface after ca. 18 h and grows on a polyether surface after ca. 28 h. The previous polyester surface resists BSA well until ca. 38 h, and the surfaces prepared in this work resist BSA very well until at least 50 h. The outstanding resistance to BSA adsorption ability arises from hydrophilicity, degradability, and longer lifetime of the film. It is observed that there is always 2 nm of protein adsorbed on all surfaces after immersion in the BSA solutions, and it is likely reversibly attached,[13,30] possibly in a dynamic equilibrium.[31]

Bicinchoninic Acid (BCA) Protein Assay. The BSA adsorption on thicker films (~4 μm) were investigated using a BCA assay. The 20 mg/mL polyester with 5% cross-linker solution was drop-casted on a BP-silicon wafer and UV-cross-linked to make films (ca. 4 μm). For comparison, the polymethyl methacrylate (PMMA) and polystyrene (PS) films were also prepared by the same method. All samples were immersed in 3 mg/mL BSA stock solution for 24 h. The specimens were then taken out, and the amounts of adsorbed protein were quantified by a BCA assay. The calculated adsorbed BSA amount for each sample are summarized in Figure 7. The results show that the polyester films only adsorb 2.31 μg/cm^2 BSA, much less than the BSA adsorbed on PS, PMMA, and polyether films. This experiment reconfirms the BSA resistance ability of the synthesized polyester films.

Characterization of Film Hydration and Surface Hydrophilicity. In addition to resisting protein via degradation of the network, the film hydration and surface hydro-

https://doi.org/10.1021/acs.langmuir.1c02822
Langmuir 2022, 38, 1488−1496

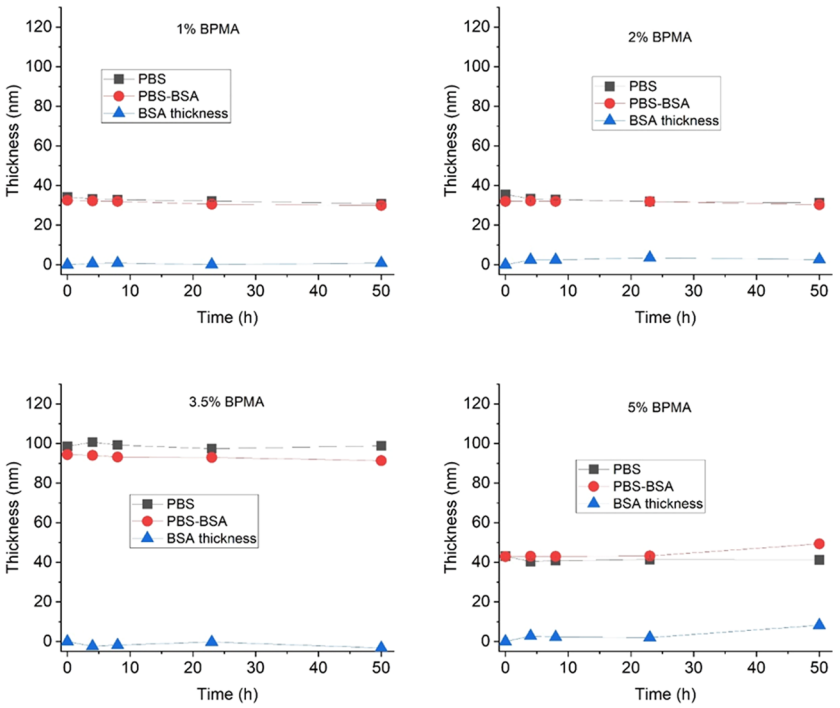

Figure 5. Plots showing the thickness of thin films with various BPMA ratios immersed in BSA-PBS solution (ionic strength 100 mM, pH 7.4, BSA 3 mg/mL) for various times. Thicknesses of the films were obtained via ellipsometry. All data points were the average values of three measurements on different locations of the same sample, and error bars represent one standard deviation of the average. Many error bars were smaller than the size of the plot symbols.

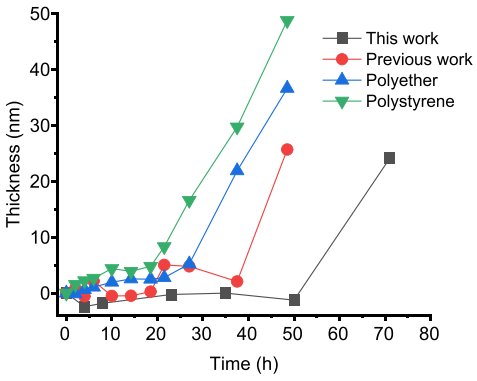

Figure 6. Plots showing calculated BSA thickness on polyester, PS, previously reported polyester film,[13] and polyether film prepared in this work.

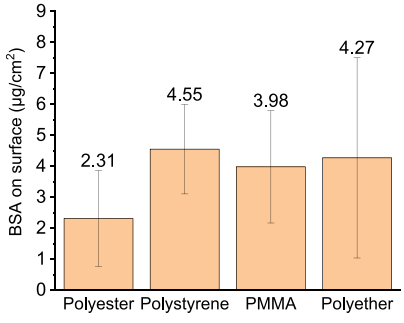

Figure 7. BSA adsorbed on different surfaces after 24 h immersion quantified by the BCA assay. Each data is the average value of six measurements on different samples. The chemical structure of the polyester is shown in Scheme 1; the chemical structure of polyether is shown in Figure S11.

philicity may also influence protein adsorption.[32] Therefore, the swelling ratio of spin-coating films in deionized water and water contact angle of films were measured.

The measurement of the swelling ratio of spin-coated films followed the procedure in the literature.[30] After washing by THF, the "dry" thickness of the film was measured. Then, the sample was immersed in DI water and left for 1 min to reach equilibrium. The thickness of the film in water was measured and marked as d_{wet}. The swelling ratio of the film (α) was calculated as

$$\alpha = \frac{d_{wet}}{d_{dry}} \tag{5}$$

Figure 8 plots the relationship between the swelling ratio and gel fractions. The degree of swelling is strongly affected by the gel fraction of the network. The swelling ratio increases

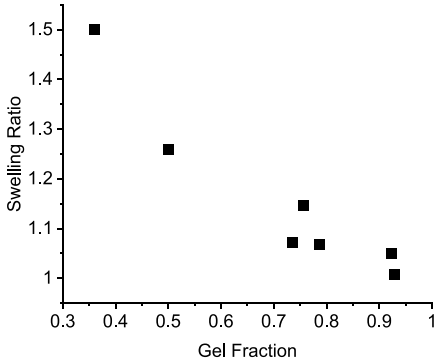

Figure 8. Swelling ratio of spin-coating films of polyesters synthesized (Scheme 1) with different gel fractions.

https://doi.org/10.1021/acs.langmuir.1c02822
Langmuir 2022, 38, 1488−1496

proportionally with decreasing gel fraction, indicating that the hydration is greater for lower gel fraction networks. The swelling ratio affects protein adsorption by "entropic shielding".[30] Genzer and Pandiyarajan pointed out that fibrinogen (Fg) adsorption on hydrogel substrates was influenced by the degree of cross-linking and the swelling capacity of networks.[30] They proposed that the enthalpy contribution to the protein adsorption process is negligible for hydrophilic coatings. Therefore, the entropy change dominates the Gibbs free energy of adsorption process. Moreover, the entropy loss due to reduced freedom of the swollen chains overcomes the increasing entropy from the mix of protein and network. The higher swelling ratio of networks with lower gel fractions indicates more degrees of freedom, and thus the system needs to sacrifice more entropy for protein adsorption. Therefore, the protein adsorption on highly swollen networks is entropically less favorable than on less swollen networks.

The swelling ratio of drop-casting films was also measured. A piece of free-standing film was weighed and immersed in water for 2 h to reach equilibrium. The solvent was removed by a micro-pipette, and the new weight was recorded until the weight variation was <0.5%. The swelling ratio of bulk gels was calculated as shown in eq 6.[30]

$$\alpha_{3D}^{bulk} = \left(\frac{V_{polymer} + V_{solvent}}{V_{polymer}}\right) = \left(1 + \frac{m_{solvent}}{m_{polymer}}\frac{\rho_{polymer}}{\rho_{solvent}}\right) \quad (6)$$

In eq 2, $m_{solvent}$ and $m_{polymer}$ represent the masses of the solvent and the polymer, respectively, and $\rho_{polymer}$ (1.18 g/mL) and $\rho_{solvent}$ (1 g/mL) indicate the densities of the polymer and solvent, respectively.[30] The calculated swelling ratio of the sample with 0.8 gel fraction in water is 1.05, which is close to the result of spin-coating films. The thickness of the film does not have large influence on the hydration of the film.

Contact Angle Measurements. To judge the hydrophilicity of the spin-coating thin films with different gel fractions, they were characterized by water contact angle measurements. Figure S22 summarizes water contact angles of films with varying gel fractions. The static water contact angles are in the range of 67 to 73°, meaning all the surfaces are relatively hydrophilic. There is no obvious relationship between the water contact angle and gel fraction. Although different gel fraction films contain various BPMA ratios, they do not have pronounced influences on the hydrophilicity of the overall polymer due to the alkyl-bonded backbone of polymers.

CONCLUSIONS

Novel, degradable, anti-biofouling polyester coatings with different gel fractions were prepared by spin-coating and drop-casting. The degradation, protein adsorption behavior, hydrophilicity, and hydration of the films were investigated. The resistance to BSA adsorption of those coatings is better than PS and a hydrophilic polyether. By adjusting the cross-linker ratio in the polyester, the lifetime and swelling ratio of the coatings can be controlled. Compared with polyesters synthesized by ring-opening polymerization, the polyesters synthesized in this work achieve higher molecular weights and thicker films are prepared. Thus, these films are viable for longer periods of time.

ASSOCIATED CONTENT

Supporting Information

The Supporting Information is available free of charge at https://pubs.acs.org/doi/10.1021/acs.langmuir.1c02822.

Schemes for the synthesis of molecules and polymers prepared,prepared; ^{1}H and ^{13}C NMR data of molecules and polymers prepared, description of the reactivity ratio analysis, and supporting data for polymerization, cross-linking, degradation, and protein adsorption. (PDF)

AUTHOR INFORMATION

Corresponding Author

Christopher B. Gorman − *Department of Chemistry, North Carolina State University, Raleigh, North Carolina 27695-8204, United States;* orcid.org/0000-0001-7367-2965; Email: cbgorman@ncsu.edu

Authors

Gaoyan Mu − *Department of Chemistry, North Carolina State University, Raleigh, North Carolina 27695-8204, United States*

Jan Genzer − *Department of Chemical & Biomolecular Engineering, North Carolina State University, Raleigh, North Carolina 27695-7905, United States*

Complete contact information is available at: https://pubs.acs.org/10.1021/acs.langmuir.1c02822

Notes

The authors declare no competing financial interest.

ACKNOWLEDGMENTS

J.G. appreciates partial support from a National Science Foundation grant DMR-1809453. This work was performed in part by the Molecular Education, Technology and Research Innovation Center (METRIC) at NC State University, which is supported by the State of North Carolina. Part of this work was also performed in part at the Analytical Instrumentation Facility (AIF) at North Carolina State University, which is supported by the State of North Carolina and the National Science Foundation (award number ECCS-2025064). The AIF is a member of the North Carolina Research Triangle Nanotechnology Network (RTNN), a site in the National Nanotechnology Coordinated Infrastructure (NNCI).

REFERENCES

(1) Xu, J.; Lee, H. Anti-Biofouling Strategies for Long-Term Continuous Use of Implantable Biosensors. *Chemosensors* **2020**, *8*, 66.

(2) Prateeksha, P.; Bajpai, R.; Rao, C. V.; Upreti, D. K.; Barik, S. K.; Singh, B. N. Chrysophanol-Functionalized Silver Nanoparticles for Anti-Adhesive and Anti-Biofouling Coatings to Prevent Urinary Catheter-Associated Infections. *ACS Appl. Nano Mater.* **2021**, *4*, 1512−1528.

(3) Yu, K.; Alzahrani, A.; Khoddami, S.; Cheng, J. T. J.; Mei, Y.; Gill, A.; Luo, H. D.; Haney, E. F.; Hilpert, K.; Hancock, R. E. W.; Lange, D.; Kizhakkedathu, J. N. Rapid Assembly of Infection-Resistant Coatings: Screening and Identification of Antimicrobial Peptides Works in Cooperation with an Antifouling Background. *ACS Appl. Mater. Interfaces* **2021**, *13*, 36784−36799.

(4) Bixler, G. D.; Bhushan, B. Biofouling: lessons from nature. *Phil. Trans. R. Soc. A* **2012**, *370*, 2381−2417.

(5) Kousar, F.; Malmström, J.; Swift, S.; Ross, J.; Perera, J.; Moratti, S. C. Protein-Resistant Behavior of Poly(ethylene glycol)-Containing

Polymers with Phosphonate/Phosphate Units on Stainless Steel Surfaces. *ACS Appl. Polym. Mater.* **2021**, *3*, 2785−2801.
(6) Hu, P.; Xie, Q.; Ma, C.; Zhang, G. Silicone-Based Fouling-Release Coatings for Marine Antifouling. *Langmuir* **2020**, *36*, 2170−2183.
(7) Xu, B.; Liu, Y.; Sun, X.; Hu, J.; Shi, P.; Huang, X. Semifluorinated Synergistic Nonfouling/Fouling-Release Surface. *ACS Appl. Mater. Interfaces* **2017**, *9*, 16517−16523.
(8) Sun, X.; Wu, C.; Hu, J.; Huang, X.; Lu, G.; Feng, C. Antifouling Surfaces Based on Fluorine-Containing Asymmetric Polymer Brushes: Effect of Chain Length of Fluorinated Side Chain. *Langmuir* **2019**, *35*, 1235−1241.
(9) Lin, X.; Jain, P.; Wu, K.; Hong, D.; Hung, H.-C.; O'Kelly, M. B.; Li, B.; Zhang, P.; Yuan, Z.; Jiang, S. Ultralow Fouling and Functionalizable Surface Chemistry Based on Zwitterionic Carboxybetaine Random Copolymers. *Langmuir* **2019**, *35*, 1544−1551.
(10) Brown, M. U.; Triozzi, A.; Emrick, T. Polymer Zwitterions with Phosphonium Cations. *J. Am. Chem. Soc.* **2021**, *143*, 6528−6532.
(11) Guo, H.; Chen, P.; Tian, S.; Ma, Y.; Li, Q.; Wen, C.; Yang, J.; Zhang, L. Amphiphilic Marine Antifouling Coatings Based on a Hydrophilic Polyvinylpyrrolidone and Hydrophobic Fluorine−Silicon-Containing Block Copolymer. *Langmuir* **2020**, *36*, 14573−14581.
(12) Xu, L.; Crawford, K.; Gorman, C. B. Effects of Temperature and pH on the Degradation of Poly(lactic acid) Brushes. *Macromolecules* **2011**, *44*, 4777−4782.
(13) Mu, G.; Pandiyarajan, C. K.; Lu, X.; Weaver, M.; Genzer, J.; Gorman, C. B. Dynamic Surfaces—Degradable Polyester Networks that Resist Protein Adsorption. *Langmuir* **2021**, *37*, 8978−8988.
(14) Xu, Y.-C.; Ren, W.-M.; Zhou, H.; Gu, G.-G.; Lu, X.-B. Functionalized Polyesters with Tunable Degradability Prepared by Controlled Ring-Opening (Co)polymerization of Lactones. *Macromolecules* **2017**, *50*, 3131−3142.
(15) Saito, T.; Aizawa, Y.; Yamamoto, T.; Tajima, K.; Isono, T.; Satoh, T. Alkali Metal Carboxylate as an Efficient and Simple Catalyst for Ring-Opening Polymerization of Cyclic Esters. *Macromolecules* **2018**, *51*, 689−696.
(16) Longo, J. M.; Sanford, M. J.; Coates, G. W. Ring-Opening Copolymerization of Epoxides and Cyclic Anhydrides with Discrete Metal Complexes: Structure-Property Relationships. *Chem. Rev.* **2016**, *116*, 15167−15197.
(17) DiCiccio, A. M.; Coates, G. W. Ring-opening copolymerization of maleic anhydride with epoxides: a chain-growth approach to unsaturated polyesters. *J. Am. Chem. Soc.* **2011**, *133*, 10724−10727.
(18) Ji, H.-Y.; Wang, B.; Pan, L.; Li, Y.-S. Lewis pairs for ring-opening alternating copolymerization of cyclic anhydrides and epoxides. *Green Chem.* **2018**, *20*, 641−648.
(19) Hu, X.; Gorman, C. B. Resisting protein adsorption on biodegradable polyester brushes. *Acta Biomater.* **2014**, *10*, 3497−3504.
(20) Hill, M. R.; Guégain, E.; Tran, J.; Figg, C. A.; Turner, A. C.; Nicolas, J.; Sumerlin, B. S. Radical Ring-Opening Copolymerization of Cyclic Ketene Acetals and Maleimides Affords Homogeneous Incorporation of Degradable Units. *ACS Macro Lett.* **2017**, *6*, 1071−1077.
(21) Wu, Q.; Qu, B. Photoinitiating characteristics of benzophenone derivatives as new initiators in the photocrosslinking of polyethylene. *Polym. Eng. Sci.* **2001**, *41*, 1220−1226.
(22) Shiro Kobayashi, K. M., *Encyclopedia of Polymeric Nanomaterials*; Springer-Verlag Berlin Heidelberg: 2015, *2672*.
(23) Kazemi, N.; Duever, T. A.; Penlidis, A. Demystifying the estimation of reactivity ratios for terpolymerization systems. *AIChE J.* **2014**, *60*, 1752.
(24) Scott, A. J.; Penlidis, A. Binary vs. ternary reactivity ratios: Appropriate estimation procedures with terpolymerization data. *Eur. Polym. J.* **2018**, *105*, 442−450.
(25) Pujari, N. S.; Wang, M.; Gonsalves, K. E. Co and terpolymer reactivity ratios of chemically amplified resists. *Polymer* **2017**, *118*, 201−214.
(26) Yu, L.; Hou, Y.; Cheng, C.; Schlaich, C.; Noeske, P.-L. M.; Wei, Q.; Haag, R. High-Antifouling Polymer Brush Coatings on Nonpolar Surfaces via Adsorption-Cross-Linking Strategy. *ACS Appl. Mater. Interfaces* **2017**, *9*, 44281−44292.
(27) Hu, X.; Hu, G.; Crawford, K.; Gorman, C. B. Comparison of the growth and degradation of poly(glycolic acid) and poly(ε-caprolactone) brushes. *J. Polym. Sci., Part A: Polym. Chem.* **2013**, *51*, 4643−4649.
(28) Bratek-Skicki, A.; Eloy, P.; Morga, M.; Dupont-Gillain, C. Reversible Protein Adsorption on Mixed PEO/PAA Polymer Brushes: Role of Ionic Strength and PEO Content. *Langmuir* **2018**, *34*, 3037−3048.
(29) Jeyachandran, Y. L.; Mielczarski, E.; Rai, B.; Mielczarski, J. A. Quantitative and Qualitative Evaluation of Adsorption/Desorption of Bovine Serum Albumin on Hydrophilic and Hydrophobic Surfaces. *Langmuir* **2009**, *25*, 11614−11620.
(30) Pandiyarajan, C. K.; Genzer, J. Effect of Network Density in Surface-Anchored Poly(N-isopropylacrylamide) Hydrogels on Adsorption of Fibrinogen. *Langmuir* **2017**, *33*, 1974−1983.
(31) Bixler, G. D.; Bhushan, B. Biofouling: lessons from nature. *Phil. Trans. R. Soc. A* **1967**, *2012*, 2381−2417.
(32) Peñaflor Galindo, T. G.; Tagaya, M. Interfacial Effect of Hydration Structures of Hydroxyapatite Nanoparticle Films on Protein Adsorption and Cell Adhesion States. *ACS Appl. Bio Mater.* **2019**, *2*, 5559−5567.

https://doi.org/10.1021/acs.langmuir.1c02822
Langmuir 2022, 38, 1488−1496